Journal of Biomechanics 49 (2016) 2383–2389

Contents lists available at ScienceDirect

Journal of Biomechanics

journal homepage: www.elsevier.com/locate/jbiomech
www.JBiomech.com

Differential ascending and descending aortic mechanics parallel aneurysmal propensity in a mouse model of Marfan syndrome

C. Bellini [a,1], A. Korneva [a,1], L. Zilberberg [b,1], F. Ramirez [c], D.B. Rifkin [b], J.D. Humphrey [a,d,*]

[a] Department of Biomedical Engineering, Yale University, New Haven, CT, USA
[b] Departments of Cell Biology and Medicine, New York University, New York, NY, USA
[c] Department of Pharmacology and Systems Therapeutics, Icahn School of Medicine at Mount Sinai, New York, NY, USA
[d] Vascular Biology and Therapeutics Program, Yale School of Medicine, New Haven, CT, USA

ARTICLE INFO

Article history:
Accepted 13 November 2015

Keywords:
Thoracic aortic aneurysm
Fibrillin-1
Elastic fiber fragmentation
Stiffness
Stress

ABSTRACT

Marfan syndrome (MFS) is a multi-system connective tissue disorder that results from mutations to the gene that codes the elastin-associated glycoprotein fibrillin-1. Although elastic fibers are compromised throughout the arterial tree, the most severe phenotype manifests in the ascending aorta. By comparing biaxial mechanics of the ascending and descending thoracic aorta in a mouse model of MFS, we show that aneurysmal propensity correlates well with both a marked increase in circumferential material stiffness and an increase in intramural shear stress despite a near maintenance of circumferential stress. This finding is corroborated via a comparison of the present results with previously reported findings for both the carotid artery from the same mouse model of MFS and for the thoracic aorta from another model of elastin-associated glycoprotein deficiency that does not predispose to thoracic aortic aneurysms. We submit that the unique biaxial loading of the ascending thoracic aorta conspires with fibrillin-1 deficiency to render this aortic segment vulnerable to aneurysm and rupture.

1. Introduction

Marfan syndrome (MFS) is an autosomal dominant connective tissue disorder that results from mutations to the gene that codes the glycoprotein fibrillin-1 (Dietz et al., 1991). Along with other glycoproteins, normal fibrillin-1 associates with elastin to form the elastic fibers that constitute the concentric laminae of central arteries and endow central arteries with their primary mechanical function – to use elastic energy that is stored during systole to augment blood flow during diastole. Importantly, normal fibrillin-1 contributes significantly to the long-term stability of elastic fibers (Marque et al., 2001), that is, to their ability to resist mechanical fatigue. Although MFS leads to ocular, skeletal, and vascular disorders, it is the predisposition to ascending aortic aneurysms that renders this disorder potentially life threatening.

It has long been thought that the aorta is stiffer in MFS, even in the absence of an aneurysm, as revealed by a decreased distensibility or an increased pulse wave velocity (Jeremy et al., 1994; Groenink et al., 1998). Increased aortic stiffness, in turn, is thought to elevate central pulse pressures and thereby increase the workload on the heart and the cyclic loading of the proximal aorta (O'Rourke and Hashimoto, 2007). The latter may represent an insidious positive feedback loop that contributes to a progressive loss of proximal aortic elasticity and thus mechanical functionality. There is, therefore, a pressing need to understand better the biomechanics of the aorta in MFS and its effects on the local mechanobiology and global pathophysiology. Toward this end, mouse models allow longitudinal studies and detailed assessments of wall mechanics and hemodynamics. Herein, we present the first detailed comparison of biaxial wall mechanics of normal and MFS aortas at the ascending and proximal descending thoracic locations.

2. Methods

2.1. Specimen preparation and testing

All animal procedures were approved by the Institutional Animal Care and Use Committee at New York University. Male mice homozygous for a hypomorphic allele of the fibrillin-1 gene (*Fbn1*$^{mgR/mgR}$) and wild-type (*WT*) littermate controls were euthanized between 8 and 9 weeks of age and the thoracic aorta was excised. Details on our methods of biaxial testing and data analysis are given elsewhere (Bellini et al., 2015; Ferruzzi et al., 2015). Briefly, each vessel was

* Corresponding author at: Department of Biomedical Engineering, Malone Engineering Center, Yale University, New Haven, CT, USA. Tel.: +1 203 432 6428; fax: +1 203 432 0030.
E-mail address: jay.humphrey@yale.edu (J.D. Humphrey).
[1] These authors contributed equally.

http://dx.doi.org/10.1016/j.jbiomech.2015.11.059
0021-9290/

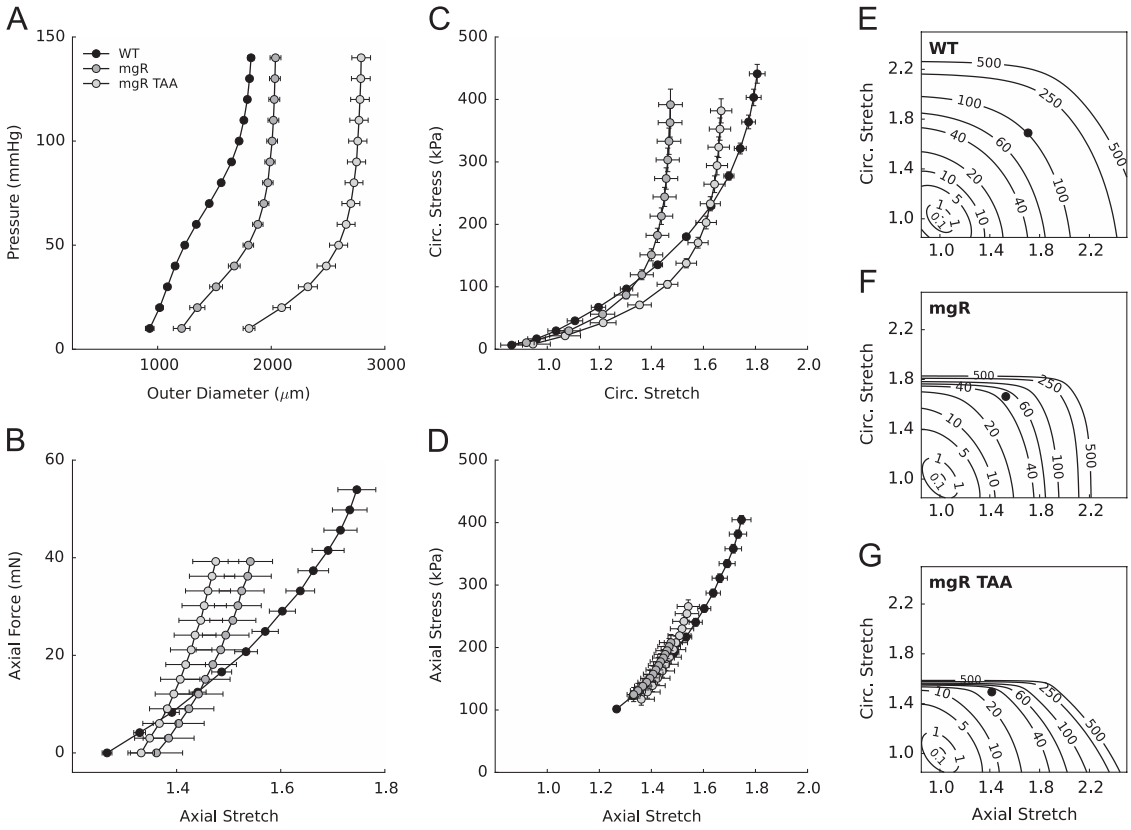

Fig. 1. Mechanical testing data (mean ± SEM) for the ascending thoracic aorta (ATA) from wild-type (black, $n=5$), non-aneurysmal *Fbn1*$^{mgR/mgR}$ (dark grey, $n=3$), and aneurysmal *Fbn1*$^{mgR/mgR}$ (light grey, $n=7$) mice. Structural responses are shown by (A) pressure-diameter curves at group-specific *in vivo* axial stretches and (B) axial force-axial stretch curves at 100 mmHg. Material responses are shown by mean (C) circumferential and (D) axial Cauchy stress–stretch curves. Iso-energy contours show elastic energy storage as a function of biaxial stretch for (E) wild-type, (F) non-aneurysmal *Fbn1*$^{mgR/mgR}$, and (G) thoracic aortic aneurysmal (TAA) *Fbn1*$^{mgR/mgR}$ ATAs; the black circles in these energy plots show the energy stored at the group-specific systolic pressure and *in vivo* axial stretch.

cleaned of peri-adventitial tissue and divided into two segments: the ascending thoracic aorta (ATA), extending from the aortic root to the brachiocephalic artery, and the descending thoracic aorta (DTA), extending from the left subclavian artery to the third pair of intercostal arteries. Branches were ligated with suture and specimens were secured on glass cannulae and placed within a custom testing system. Specimens were then chemo-mechanically acclimated for 15 minutes within a Hanks buffered solution (which minimizes smooth muscle tone) at 37 °C, while subjected to cyclic luminal pressurization (80–120 mmHg) at the approximate *in vivo* length. Thereafter, the vessels underwent standard preconditioning (Bellini et al., 2015) and were subjected to three pressure-diameter (*P-d*) and four axial force-length (*f-l*) protocols. In the former, luminal pressure was varied cyclically from 10 to 140 mmHg at three fixed axial stretches, the genotype- and location-specific *in vivo* value and ±5% of this value; in the latter, axial force was varied cyclically from ~0 to ~55 or ~40 mN for *WT* or *Fbn1*$^{mgR/mgR}$ ATAs, respectively, and ~0 to ~45 mN for the DTAs, each at four fixed values of pressure: 10, 60, 100, and 140 mmHg. Pressure, outer diameter, axial force, and axial extension were recorded on-line during each of the seven cyclic testing protocols. Unloaded wall thickness was measured using an optical coherence tomography system (ThorLabs, Newton, NJ) and verified using a dissecting microscope in rings cut from either end of the specimen.

2.2. Data analysis

Biaxial data from the unloading curves of the last recorded cycle of each of the seven *P-d* and *f-l* protocols were combined and fit simultaneously using a validated strain energy function W that accounts for the isotropic contribution of an amorphous matrix and anisotropic effects of four families of fibers (Ferruzzi et al., 2015):

$$W(\mathbf{C},\mathbf{M}^j)=\frac{c}{2}(I_\mathbf{C}-3)+\sum_{j=1}^{4}\frac{{c_1}^j}{4{c_2}^j}\left\{exp\left[{c_2}^j({IV_\mathbf{C}}^j-1)^2\right]-1\right\}, \quad (1)$$

where c, ${c_1}^j$, and ${c_2}^j$ ($j=1,2,3,4$) are model parameters. $\mathbf{C}=\mathbf{F}^T\mathbf{F}$ is the right Cauchy-Green tensor, $\mathbf{F}$ the deformation gradient tensor, and $\mathbf{M}^j=[0, \sin{\alpha_0}^j, \cos{\alpha_0}^j]$ a unit vector in the direction of the j^{th} fiber family, with angle ${\alpha_0}^j$ computed relative to the axial direction in a reference configuration. $I_\mathbf{C}=tr(\mathbf{C})$ and ${IV_\mathbf{C}}^j=\mathbf{M}^j\bullet\mathbf{C}\mathbf{M}^j$ are coordinate invariant measures of deformation. Best-fit values of the 8 model parameters were estimated using a nonlinear regression that minimized the sum-of-the-squares of the differences between computed and measured pressures and axial forces (Bellini et al., 2015). Biaxial Cauchy stress and material stiffness were calculated at paired circumferential and axial stretches and so too the stored elastic energy. Comparison of loading and unloading curves allowed energy dissipation to be estimated as a percentage of energy stored while loading. Differences between genotypes (*WT* vs. *Fbn1*$^{mgR/mgR}$) were evaluated using a Student's t-test. Differences among phenotypes (*WT* controls vs. non-aneurysmal or aneurysmal *Fbn1*$^{mgR/mgR}$) were assessed with a one-way ANOVA. Statistical significance was set at $p<0.05$. For notational simplicity, we denote *Fbn1*$^{mgR/mgR}$ mice as *mgR/mgR* below.

3. Results

All *mgR/mgR* mice die prematurely due to ruptured thoracic aortic aneurysms, but the time-course of disease progression is heterogeneous

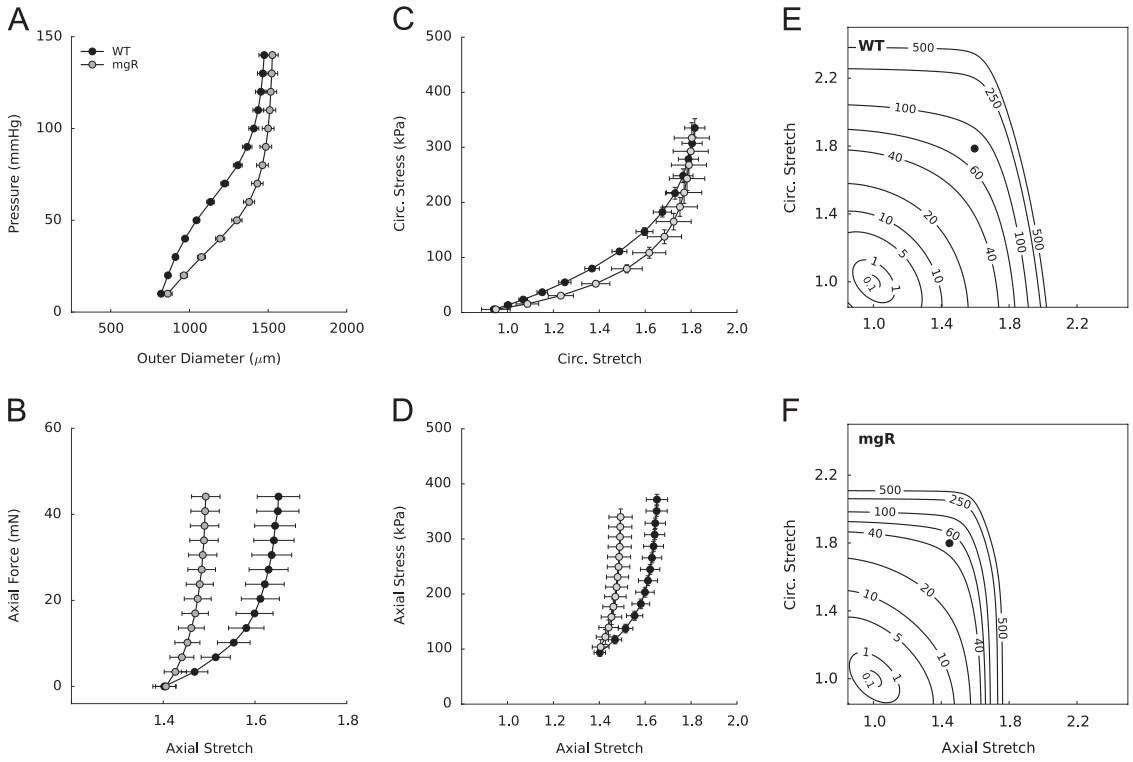

Fig. 2. Mechanical testing data (mean ± SEM) for the descending thoracic aorta (DTA) from wild-type (black, $n=5$) and *Fbn1*$^{mgR/mgR}$ (grey, $n=8$) mice. Structural responses are shown by (A) pressure-diameter curves at group-specific *in vivo* axial stretches and (B) axial force-axial stretch curves at 100 mmHg. Material responses are shown by mean (C) circumferential and (D) axial Cauchy stress – stretch curves. Iso-energy contours show elastic energy storage as a function of biaxial stretch for (E) wild-type and (F) *Fbn1*$^{mgR/mgR}$ DTAs; the black circles in these energy plots show the energy stored at the group-specific systolic pressure and *in vivo* axial stretch.

(Cook et al., 2015). Indeed, upon excision and mechanical analysis, ATAs from *mgR/mgR* mice separated naturally into two groups: non-aneurysmal with a 19% mean dilatation of the unloaded outer diameter ($n=3$) and aneurysmal with a 76% mean dilatation ($n=7$). The former group represents an early, pre-aneurysmal stage at 8 to 9 weeks of age, which presumably would have become aneurysmal at an older age. We compared both groups separately with ATAs from the *WT* mice ($n=5$). DTAs were compared simply by genotype, *WT* ($n=5$) and *mgR/mgR* ($n=8$), since there was no correlation between DTA behavior and the presence of an ATA aneurysm.

Pressure-diameter responses at individual values of *in vivo* axial stretch were qualitatively similar for the two regions (ATA vs. DTA) for the *WT* and non-aneurysmal *mgR/mgR* groups (Figs. 1–2, A). While a clear change in curvilinearity is visible for both *WT* groups, this characteristic is reduced in the non-aneurysmal *mgR/mgR* groups and lost in the aneurysmal *mgR/mgR* ATAs. This observation suggests an earlier engagement of collagen fibers with a progressively compromised load bearing capability of the elastic fibers, as expected in fibrillin-1 deficiency. Accordingly, best-fit values of the neo-Hookean parameter (c) in the constitutive relation (Eq. 1), which models the nearly isotropic contribution of the elastin-dominated amorphous matrix (Eberth et al., 2009), decreases for the *mgR/mgR* mice (Table 1). Compared with the *mgR/mgR* groups, the *WT* span a wider range of axial stretches in response to the same range of axial forces for both the ATA and DTA, with luminal pressure set at 100 mmHg. Interestingly, the structural behavior of the non-aneurysmal and aneurysmal *mgR/mgR* ATAs is similar in the axial direction (Figs. 1–2, B).

Despite the overall reduced range of circumferential deformation experienced by the *mgR/mgR* ATA, plots of mean circumferential stress–stretch data confirmed a qualitative similarity in the intrinsic material, not just structural, behavior in both regions (Figs. 1–2, C). Similarly, within the common range of axial stretches, *WT* and *mgR/mgR* ATAs, both non-aneurysmal and aneurysmal, show an overlapping axial material response (Fig. 1D). The axial stress–stretch behavior in the DTA is also qualitatively similar between the *WT* and *mgR/mgR* groups, despite the lower range of axial stretches experienced by the mutants (Fig. 2D).

Nevertheless, elastic energy storage differed significantly between the two regions and between genotypes, correlating well with the loss of distensibility due to fibrillin-1 deficiency, especially in aneurysmal vessels (Figs. 1E–G, 2E–F). Whereas energy storage is generally higher in the ATA than the DTA due to its greater biaxial loading *in vivo*, loss of energy storage was particularly dramatic in the ATA (from 119 kPa in *WT* to 59 and 43 kPa, respectively, in non-aneurysmal and aneurysmal *mgR/mgR* vessels) compared with that in the DTA (from 78 in *WT* to 49 kPa in *mgR/mgR*), when calculated at genotype-specific systolic pressures: 124 mmHg for *WT* and 131 mmHg for *mgR/mgR* (Marque et al., 2001). Energy dissipation also increased with fibrillin-1 deficiency, from ~2.1 to 5.5% in the ATA and from 4.0 to 7.6% in the DTA.

Figs. 3 and 4 highlight further geometric (panels A,B), material (C–F), and structural (G,H) differences at individual *in vivo* conditions by region and genotype. Fibrillin-1 deficiency resulted in a consistent decrease in the preferred *in vivo* value of axial stretch, from 1.70 (*WT*) to 1.52 (non-aneurysmal) and 1.42 (aneurysmal) in ATAs and from 1.60 to 1.44 in DTAs (Figs. 3–4, A). Increases in wall thickness of the *mgR/mgR* aortas (Figs. 3–4, B) nevertheless appeared to offset differences in diameter (Figs. 1–2, A) such that mean values of circumferential wall stress were similar between genotypes (Figs. 3–4, C), though higher in ATA than in DTA: 382 kPa in *WT* vs. 361 kPa (non-aneurysmal) and 369 kPa (aneurysmal) in *mgR/mgR* ATAs, and 293 kPa in *WT* vs. 291 kPa in *mgR/mgR* DTAs. The axial stresses were yet significantly lower in all fibrillin-1 deficient aortas (Figs. 3–4, D): 395 kPa in *WT* vs. 260 kPa (non-aneurysmal) and 218 kPa (aneurysmal) in *mgR/mgR* ATAs, and 272 vs. 194 kPa in *WT* and *mgR/mgR* DTAs, likely due in large part to the reduced axial stretches (Figs. 1–2, B and D). Maximum in-plane shear stress, calculated as one-half of the difference between circumferential and axial (principal) stresses, was significantly greater in fibrillin-1 deficient aortas independent of region:

Table 1
Best-fit values of model parameters for the microstructurally motivated strain energy function in Eq. 1 at each anatomical location and for each experimental group. Wild-type (*WT*), non-aneurysmal *Fbn1*$^{mgR/mgR}$ (*mgR*), and aneurysmal *Fbn1*$^{mgR/mgR}$ (*mgR* TAA) vessels were compared in the ascending thoracic aorta (ATA). Wild-type (*WT*) and *Fbn1*$^{mgR/mgR}$ (*mgR*) vessels were compared in the descending thoracic aorta (DTA).

	Elastic Fibers	Axial Collagen		Circumferential Collagen + SMC		Symmetric Diagonal Collagen			Error
	c (kPa)	c_1^1 (kPa)	c_2^1	c_1^2 (kPa)	c_2^2	$c_1^{3,4}$ (kPa)	$c_2^{3,4}$	α_0 (deg)	*RMSE*
ATA									
WT	43.99	14.98	0.03	7.59	0.23	6.48	0.43	44	0.048
mgR	23.10	12.99	0.23	0.01	2.39	7.48	0.75	47	0.068
mgR TAA	21.69	11.14	0.01	8.44E-05	8.29	11.14	1.56	54	0.092
DTA									
WT	31.94	13.50	0.16	11.21	0.15	0.10	1.82	27	0.054
mgR	29.04	1.29	1.78	1.14	0.58	0.34	2.38	29	0.084

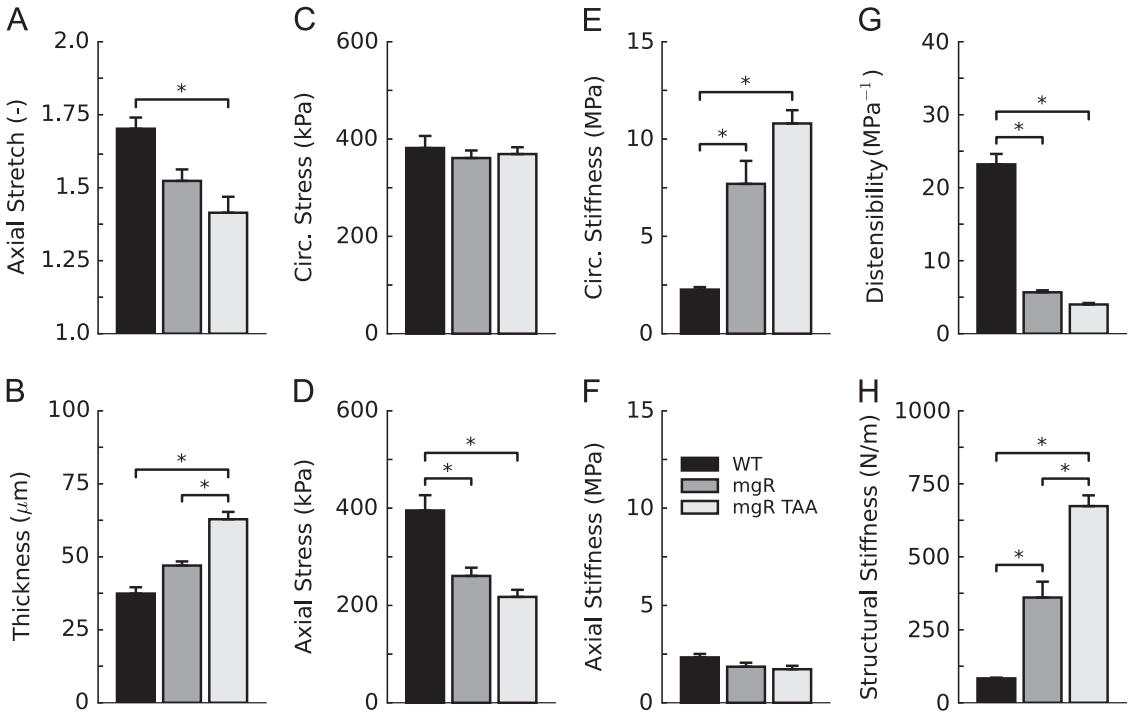

Fig. 3. Comparison of geometric, material, and structural metrics among wild-type (black, $n=5$), non-aneurysmal *Fbn1*$^{mgR/mgR}$ (dark grey, $n=3$), and aneurysmal *Fbn1*$^{mgR/mgR}$ (light grey, $n=7$) ascending thoracic aortas (ATAs) at group-specific systolic pressure (mean ± SEM). (A) In vivo axial stretch, (B) wall thickness, mean (C) circumferential and (D) axial wall stress, mean (E) circumferential and (F) axial material stiffness, (G) distensibility, and (H) circumferential structural stiffness. Statistical significance (*) assessed by one-way ANOVA with $p<0.05$.

~13 kPa in *WT* vs. 50 kPa (non-aneurysmal) and 76 kPa (aneurysmal) in *mgR/mgR* ATAs, and ~15 vs. 48 kPa in *WT* and *mgR/mgR* DTAs.

Intrinsic material stiffness increased significantly in the circumferential direction due to fibrillin-1 deficiency, particularly in ATAs (Figs. 3–4, E): from 2.27 MPa in *WT* to 7.70 MPa (non-aneurysmal) and 10.8 MPa (aneurysmal) in *mgR/mgR* ATAs and from 1.77 MPa in *WT* to 3.82 MPa in *mgR/mgR* DTAs. In contrast, consistent with the reduced axial stretch, there was a trend toward decreased axial material stiffness due to fibrillin-1 deficiency (Figs. 3–4, F): from 2.33 MPa in *WT* to 1.85 MPa (non-aneurysmal) and 1.72 (aneurysmal) in *mgR/mgR* ATAs and from 3.73 in *WT* to 3.38 MPa in *mgR/mgR* DTAs. Overall circumferential structural stiffness was also greater in ATAs and DTAs due to fibrillin-1 deficiency (Figs. 3–4, H). Distensibility consistently followed the opposite trend (Figs. 3–4, G).

4. Discussion

It has long been thought that the entire aorta tends to be stiffer in MFS, yet the propensity to aneurysmal enlargement manifests in the ascending region alone, often starting at the aortic root (Jeremy et al., 1994; Groenink et al., 1998; Jondeau et al., 1999). The present findings of differential ascending and descending aortic mechanics are consistent with these basic observations, but provide the most detailed comparison to date of quantifiable biaxial structural and material properties in the thoracic aorta in an established mouse model.

A primary function of the proximal aorta is to store energy elastically during systole and to use this energy to work on the blood during diastole (Faury, 2001; Ferruzzi et al., 2015). One of the most dramatic differences in fibrillin-1 deficient aortas was the loss of energy storage capability (Figs. 1E–G, 2E–F), that is, a compromised mechanical functionality. Loss of energy storage typically results from one of two changes (Bersi et al., 2014): loss of elastic fiber integrity, which reduces the ability of these fibers to store energy, or increased fibrillar collagen, which prevents the wall from distending and thereby limits the deformation of competent elastic fibers. The latter is common in hypertension, but *mgR/mgR* mice have only modestly increased blood pressures and they have either near normal or compromised collagen (Marque et al., 2001; Ju et al., 2014). Hence, the reduced ability of *mgR/mgR* aortas to store energy stems from the

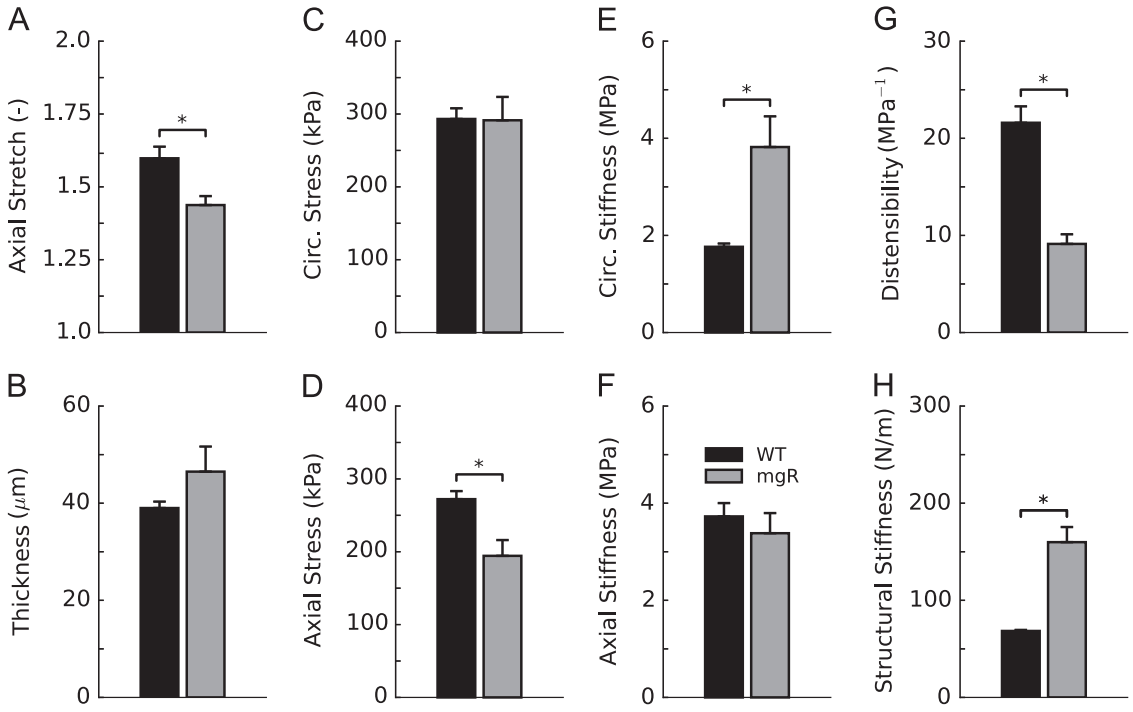

Fig. 4. Comparison of geometric, material, and structural metrics among wild-type (black, $n=5$) and *Fbn1*$^{mgR/mgR}$ (grey, $n=8$) descending thoracic aortas (DTAs) at group-specific systolic pressure (mean ± SEM). (A) In vivo axial stretch, (B) wall thickness, mean (C) circumferential and (D) axial wall stress, mean (E) circumferential and (F) axial material stiffness, (G) distensibility, and (H) circumferential structural stiffness. Statistical significance (*) assessed by Student's t-test with $p<0.05$.

impaired long-term stability of the elastic fibers in the absence of fibrillin-1 (Ramirez et al., 2007). Recently, we studied the fibulin-5 null mouse (*Fbln5*$^{-/-}$), which is another model of compromised elastic fiber integrity, though due to impaired elastogenesis (Ferruzzi et al., 2015). Comparison of the present results with those for the *Fbln5*$^{-/-}$ mouse reveals some remarkable similarities. ATAs from *WT* mice in these two studies have mean values of *in vivo* elastic energy storage of 119 kPa (at 124 mmHg) and 109 kPa (at 120 mmHg), respectively, whereas the corresponding mutants had mean values of 59 kPa (non-aneurysmal *mgR/mgR*), 43 kPa (aneurysmal *mgR/mgR*), and 43 kPa (*Fbln5*$^{-/-}$). Interestingly, the mean axial stretch for the ATAs was 1.70 (*Fbn1*$^{+/+}$) and 1.71 (*Fbln5*$^{+/+}$) for the *WT*s, and 1.52 (non-aneurysmal *mgR/mgR*), 1.42 (aneurysmal *mgR/mgR*), and 1.54 (*Fbln5*$^{-/-}$) for the mutants. The associated mean circumferential stretch was 1.78 and 1.77 for the *WT*s, and 1.67 (non-aneurysmal *mgR/mgR*), 1.50 (aneurysmal *mgR/mgR*), and 1.58 (*Fbln5*$^{-/-}$) for the mutants. These results confirm an adverse consequence of reduced elastic fiber integrity, regardless of the molecular cause, and emphasize the importance of biaxial mechanics. Given that stored energy depends directly on biaxial stretches, our results suggest that clinical assessments of the overall mechanical functionality of the ATA should include distension and extension. Fortunately, such measurements are straightforward clinically using non-invasive imaging.

Notwithstanding some similarities, one would expect differences in wall mechanics between *mgR/mgR* and *Fbln5*$^{-/-}$ mice due to the specific contributions of fibrillin-1 and fibulin-5 to elastic fiber integrity. Material stiffness is an indicator of how stress increases in response to increases in strain. Remarkably, values of material stiffness in the ATA of *Fbln5*$^{-/-}$ mice were similar to those of *WT* controls while the associated biaxial wall stress was lower due to the reduced *in vivo* stretches (Ferruzzi et al., 2015); both of these findings should protect a fibulin-5 compromised wall from acute pressure-induced mechanical damage. Indeed, aneurysms do not form in fibulin-5 deficient mice, even with induced hypertension (unpublished results). In stark contrast, although biaxial wall stress was also similar to (circumferential) or lower than (axial) normal in *mgR/mgR* ATAs (Fig. 3C–D), due to the reduced axial stretch, increased wall thickness, and a larger diameter in the mutant arteries (Fig. 3A–B, Fig. 1A), the circumferential material stiffness was dramatically higher in the *mgR/mgR* ATA (3.4-fold in the non-aneurysmal group and 4.8-fold in the aneurysmal group, noting that the non-aneurysmal group would likely become aneurysmal in time). In other words, any acute pressure-induced increase in distension would likely increment the circumferential stress significantly, which could render the ATA increasingly susceptible to mechanical damage in fibrillin-1 deficiency.

Importantly, the additional ~40% increase in circumferential material stiffness as the *mgR/mgR* ATAs became aneurysmal is consistent with a progressive loss of elastic fiber integrity with increased dilatation. This stiffening is also consistent with straighter collagen fibers in fibrillin-1 deficiency (Ju et al., 2014), not unlike that which results from elastase treatment (Ferruzzi et al., 2011). Interestingly, the circumferential stiffness of the DTA was also elevated in the *mgR/mgR* mouse, though only ~2.2 fold. Collectively, these observations suggest that increased material stiffness, if high enough, can contribute to the development of an aneurysm, not merely be a consequence of aneurysmal dilatation. Finally, this observed regional difference in aortic mechanics is consistent with findings that elastic fibers are fragmented throughout the aorta in the *mgR/mgR* mouse, though most so in the ATA (Schwill et al., 2013). We emphasize, therefore, that the ATA, not DTA, is particularly susceptible to aneurysmal dilation and mechanical failure by dissection/rupture in mice and humans. Indeed, two of the seven mice in the aneurysmal *mgR/mgR* group died from a ruptured ATA.

Although roles of in-plane shear stress in dissection/rupture are not known, our results suggest that there is a need to consider such roles, particularly given the layered structure of the aortic media. The in-plane shear stress was ~1.5-fold higher in aneurysmal (76 kPa) than in non-aneurysmal (50 kPa) *mgR/mgR* ATAs, both of which were dramatically higher than values in *WT* controls (13 kPa). Collectively, an increased circumferential material stiffness and increasingly non-equibiaxial wall stress in the ATA may

render it particularly vulnerable to acute increases in pressure. This possibility is consistent with the clinical recommendation that Marfan patients avoid strenuous activities that increase blood pressure acutely, especially weight lifting (Elefteriades and Farkas, 2010). Indeed, because fibrillin-1 contributes to the long-term stability of the elastic fibers, future studies should assess whether this increase in stiffness progresses with age (biological vs. chronological), as expected of mechanical fatigue in cyclic loading.

Whereas outer diameter under *in vivo* loading was < 5% higher in the *mgR/mgR* DTA in comparison to control, it was ~14% (non-aneurysmal) and ~55% (aneurysmal) higher in the *mgR/mgR* ATA. Computational growth and remodeling models show that aneurysmal expansion can proceed from highly local losses of elastic fiber integrity and that the aneurysmal wall tends to become circumferentially stiffer due to a turnover of collagen having a preferred orientation toward circumferential (Wilson et al., 2013). Our findings of progressive increases in circumferential stiffness are consistent with these model predictions, but there is a need for a detailed 3-D histological quantification of collagen organization within different regions of an aneurysmal vessel. Regardless, that the measured increase in circumferential stiffness (3.4 fold) in the non-aneurysmal ATAs preceded expansion suggests that subsequent turnover of collagen will exacerbate the increase in stiffness, not initiate it, even if this is a failed attempt by the cells to limit the expansion.

To our knowledge, the present data represent the first detailed biaxial study of the mechanical properties of the aorta in any animal model of MFS. There are, however, a few prior studies of mechanical properties. Aneurysmal ATAs in $Fbn1^{C1039G/+}$ mice appear to exhibit a lower failure stress than either non-aneurysmal ATAs or aged-matched controls (Chung et al., 2007). We did not measure strength, hence we cannot compare our results with these findings. Their associated stress–strain data were acquired using uniaxial ring tests, however, which do not capture *in vivo* relevant biaxial behavior and thus can be misleading (Humphrey, 2002). Indeed, given that our data revealed that marked changes in axial stretch play fundamental roles in the mechanics, ring tests are inappropriate for studying fibrillin-1 deficiency. Carta et al. (2009) presented pressure-diameter data for $Fbn1^{+/-}$ mice and computed an incremental circumferential modulus. They report that "reducing either elastin or fibrillin-1 content increases arterial stiffness at mid to high pressures" and suggested that elastin contributes primarily to elastic recoil while fibrillin-1 provides tensile strength. Our results are consistent with this report. Finally, Haskett et al. (2012) studied non-aneurysmal DTAs in $Fbn1^{C1034G/+}$ mice. Biaxial properties were apparently measured, but information was only provided for the circumferential direction and the data were analyzed using non-conjugate stress and strain; reported values of stiffness are thus not meaningful. Although not based on direct mechanical testing, results from an early study of the *mgR/mgR* mouse (Marque et al., 2001) are nevertheless consistent with our findings. Briefly, pulse wave velocity (from the descending thoracic to the abdominal aorta) was ~1.9-fold higher in the *mgR/mgR* mouse, with a ~4-fold higher estimated wall stiffness despite similar wall stresses (cf. Fig. 4). This value is comparable to the ~2.6-fold increase in structural stiffness (material stiffness multiplied by wall thickness) that we measured directly for the DTA, which influences such measures of pulse wave velocity. We emphasize, however, that the gold standard measure of central artery stiffness, carotid-to-femoral pulse wave velocity, excludes information on the ATA, which is most important in MFS. Our measured fold increase in structural stiffness was ~7.9 in the aneurysmal *mgR/mgR* ATAs. Direct *in vivo* measurements of ATA pulse wave velocity or distensibility (cf. Groenink et al., 1998) are thus preferred in this patient population.

We previously reported biaxial data for the common carotid artery (CCA) from the *mgR/mgR* mouse (Eberth et al., 2009). A re-analysis of the data revealed that energy storage was lower in the fibrillin-1 deficient CCA even though circumferential stress and stiffness were similar to that of control (Bersi et al., 2014). Combined with the present results, these findings suggest that although stored energy is a sensitive metric of mechanical functionality, a marked increase in circumferential material stiffness of the ATA may be a better indicator of susceptibility to aneurysmal enlargement and rupture (Fig. 3E). A key question, however, is whether these different studies provide any insight into the propensity of the ATA alone to become aneurysmal or to rupture. It has been suggested, for example, that this site-specific predilection may result from the differential embryonic lineage of cells along the aorta (Ruddy et al., 2013) or differential mechanical loading (Martufi et al., 2014). Although the ATA and DTA have different cell lineages and different wall mechanics, the former being neural crest- and the latter mesoderm-derived, the ATA and CCAs share a neural crest lineage and yet have different mechanics. Given that mechanical changes are dramatic in the ATA but modest in the CCA suggests that lineage alone is not causative. A similar conclusion has been suggested in fibulin-4 deficiency (Le et al., 2014). We acknowledge, however, that aneurysms in humans tend to originate at the aortic root in MFS, where there is a transition from second heart field to neural crest lineage cells. Such transitions warrant further study. Given the significant differences among the ATA, DTA, and CCAs in arterial-wide fibrillin-1 deficiency, differential mechanical loading could yet play an important role in disease susceptibility. Amongst these three vessels, the ascending aorta alone experiences a marked biaxial loading with every cardiac cycle: blood pressure causes significant (circumferential) distensions, while contraction and shortening of the heart causes significant (axial) extensions. This cyclic biaxial loading could accelerate fatigue-related fragmentation of fibrillin-1 deficient elastic fibers, consistent with general concepts that fatigue plays an important role in aging and hypertension-related stiffening (Gosline et al., 2002) and that normal fibrillin-1 contributes to the fatigue resistance of elastic arteries (Marque et al., 2001).

In summary, consistent with diffuse elastic fiber fragmentation along the aorta, fibrillin-1 deficiency leads to a consistent increase in circumferential material and structural stiffness in the ascending and descending thoracic aorta that was not seen in common carotid arteries, which are aneurysm resistant. Such aortic stiffening is expected to adversely increase the pulse wave velocity, which could augment central pulse pressures and increase cyclic loading of the proximal aorta. Given the likely progressive increase in circumferential stiffness in the ascending aorta, a higher pulse pressure could cause wall stresses to rise, which could accelerate elastic fiber fragmentation and render the ascending aorta increasingly susceptible to aneurysmal enlargement and/or rupture due to mechanical factors and proteolytic responses. This positive feedback mechanism emphasizes the need for early intervention to prevent progressive worsening. Further complicating this degenerative loss of mechanical functionality and structural integrity is the instructional, not just structural role, of elastic fibers and their constituent glycoproteins. Diminished expression of fibrillin-1, and consequent effects on elastic fiber integrity and collagen organization, might implicate a change in mechanosensing (Humphrey et al., 2015). Therapeutic interventions should thus focus not just on reducing the mechanical stress on the matrix, but also on blocking the adverse cell signaling that can result in dysfunctional mechanoregulation of the matrix.

Conflict of Interest Statement

None to declare.

Acknowledgments

This work was supported by grants from the NIH (R01-HL105297, U01-HL116323, and P01-AR49698), a NYUMC Cancer

Center Grant (P30-CA016087), and a National Marfan Foundation Grant.

Appendix A. Supplementary material

Supplementary data associated with this article can be found in the online version at http://dx.doi.org/10.1016/j.jbiomech.2015.11.059.

References

Bellini, C., Wang, S., Milewicz, D.M., Humphrey, J.D., 2015. *Myh11*$^{R247C/R247C}$ mutations increase thoracic aortic vulnerability to intramural damage despite a general biomechanical adaptivity. J. Biomech. 48, 113–121.

Bersi, M.R., Ferruzzi, J., Eberth, J.F., Gleason, R.L., Humphrey, J.D., 2014. Consistent biomechanical phenotyping of common carotid arteries from seven different genetic, pharmacological, and surgical mouse models. Ann. Biomed. Eng. 42, 1207–1223.

Carta, L., Wagenseil, J.E., Knutsen, R.H., Mariko, B., Faury, G., Davis, E.C., Starcher, B., Mecham, R.P., Ramirez, F., 2009. Discrete contributions of elastic fiber components to arterial development and mechanical compliance. Arter. Thromb. Vasc. Biol. 29, 2083–2089.

Chung, A.W.Y., Young, K.A., Sandor, G.G.S., Judge, D.P., Dietz, H.C., van Breeman, C., 2007. Loss of elastic fiber integrity and reduction of vascular smooth muscle contraction resulting from the upregulated activities of matrix metalloproteinase-2 and -9 in the thoracic aortic aneurysm in Marfan syndrome. Circ. Res. 101, 512–522.

Cook, J.R., Clayton, N.P., Carta, L., Galatioto, J., Chiu, E., Smaldone, S., Nelson, C.A., Cheng, S.H., Wentworth, B.M., Ramirez, F., 2015. Dimorphic effects of transforming growth factor – beta signaling during aortic aneurysm progression in mice suggest a combinatorial therapy for Marfan syndrome. Arter. Thromb. Vasc. Biol. 35, 911–917.

Dietz, H.C., Cutting, C.R., Pyeritz, R.E., et al., 1991. Marfan syndrome caused by a recurrent de novo missense mutation in the fibrillin gene. Nature 352, 337–339.

Eberth, J.F., Taucer, A.I., Wilson, E., Humphrey, J.D., 2009. Mechanics of carotid arteries from a mouse model of Marfan Syndrome. Ann. Biomed. Eng. 37, 1093–1104.

Elefteriades, J.A., Farkas, E.A., 2010. Thoracic aortic aneurysm: clinically pertinent controversies and uncertainties. J. Am. Coll. Cardiol. 55, 841–857.

Faury, G., 2001. Function-structure relationship of elastic arteries in evolution: from microfibrils to elastin and elastic fibres. Pathol. Biol. 49, 310–325.

Ferruzzi, J., Collins, M.J., Yeh, A.T., Humphrey, J.D., 2011. Mechanical assessment of elastin integrity in fibrillin-1-deficient carotid arteries: implications for Marfan syndrome. Cardiovasc. Res. 92, 287–295.

Ferruzzi, J., Bersi, M.R., Uman, S., Yanagisawa, H., Humphrey, J.D., 2015. Decreased energy storage, not increased material stiffness, characterizes central artery dysfunction in fibulin-5 deficiency independent of sex. J. Biomech. Eng., 137, ePub ahead of print.

Gosline, J., Lille, M., Carrington, E., Guerette, P., Ortlepp, C., Savage, K., 2002. Elastic proteins: biological roles and mechanical properties. Philos. Trans. R. Soc. Lond. B 357, 121–132.

Groenink, M., de Roos, A., Mulder, B.J.M., Spaan, J.A.E., van der Wall, E.E., 1998. Changes in aortic distensibility and pulse wave velocity assessed with magnetic resonance imaging following beta-blocker therapy in the Marfan syndrome. Am. J. Cardiol. 82, 203–208.

Haskett, D., Doyle, J.J., Gard, C., Chen, H., Ball, C., Estabrook, M.A., Encinas, A.C., Dietz, H.C., Utzinger, U., vande Geest, J.P., Azhar, M., 2012. Altered tissue behavior of a non-aneurysmal descending thoracic aorta in the mouse model of Marfan syndrome. Cell. Tissue Res. 347, 267–277.

Humphrey, J.D., 2002. Cardiovascular Solid Mechanics: Cells, Tissues, and Organs. Springer, NY.

Humphrey, J.D., Schwartz, M.A., Tellides, G., Milewicz, D.M., 2015. Role of mechanotransduction in vascular biology: focus on thoracic aortic aneurysms and dissections. Circ. Res. 116, 1448–1461.

Jeremy, R.W., Huang, H., Hwa, J., McCarrron, H., Hughes, C.F., Richards, J.G., 1994. Relation between age, arterial distensibility, and aortic dilatation in the Marfan syndrome. Am. J. Cardiol. 74, 369–373.

Jondeau, G., Boutouyrie, P., Lacolley, P., Laloux, B., Dubourg, O., Bourdarias, J.P., Laurent, S., 1999. Central pulse pressure is a major determinant of ascending aorta dilatation in Marfan syndrome. Circulation 99, 2677–2681.

Ju, X., Ijaz, T., LeJune, W., Vargas, G., Shilagard, T., Recinos, A., Milewicz, D.M., Brasier, A.R., Tilton, R.G., 2014. IL-6 regulates extracellular matrix remodeling associated with aortic dilatation in a fibrillin-1 hypomorphic mgR/mgR mouse model of severe Marfan syndrome. J. Am. Heart Assoc. 3, e000476.

Le, V.P., Yamashiro, Y., Yanagisawa, H., Wagenseil, J.E., 2014. Measuring, reversing, and modeling the mechanical changes due to the absence of fibulin-4 in mouse arteries. Biomech. Model. Mechanobiol. 13, 1081–1095.

Marque, V., Kieffer, P., Gayraud, B., Lartaud-Idjouadiene, I., Ramirez, F., Atkinson, J., 2001. Aortic wall mechanics and composition in a transgenic mouse model of Marfan syndrome. Arter. Thromb. Vasc. Biol. 21, 1184–1189.

Martufi, G., Gasser, T.C., Appoo, J.J., Di Martino, E.S., 2014. Mechanobiology in the thoracic aortic aneurysm: a review and case study. Biomech. Model. Mechanobiol. 13, 917–928.

O'Rourke, M.F., Hashimoto, J., 2007. Mechanical factors in arterial aging: a clinical perspective. J. Am. Coll. Cardiol. 50, 1–13.

Ramirez, F., Sakai, L.Y., Rifkin, D.B., Dietz, H.C., 2007. Extracellular microfibrils in development and disease. Cell. Mol. Life Sci. 64, 2437–2446.

Ruddy, J.M., Jones, J.A., Ikonimidis, J.S., 2013. Pathophysiology of thoracic aortic aneurysm (TAA): is it not one uniform aorta? Role of embryonic origin. Prog. Cardiovasc. Dis. 56, 68–73.

Schwill, S., Seppelt, P., Grunhagen, J., Ott, C.-E., Jugold, M., Ruhparwar, A., Robinson, P.N., Karck, M., Kallenbach, K., 2013. The fibrillin-1 hypomorphic mgR/mgR murine model of Marfan syndrome shows severe elastolysis in all segments of the aorta. J. Vasc. Surg. 57, 1628–1636.

Wilson, J.S., Baek, S., Humphrey, J.D., 2013. Parametric study of effects of collagen turnover in human abdominal aortic aneurysms. Proc. R. Soc. A 469, 20120556.